Dalton Transactions



COMMUNICATION

View Article Online
View Journal | View Issue



Cite this: *Dalton Trans.*, 2019, **48**,

Received 10th September 2018, Accepted 30th November 2018 DOI: 10.1039/c8dt03653e

rsc.li/dalton



Anurag Kawde, ^[] Alagappan Annamalai, ^[] Anita Sellstedt, ^d Pieter Glatzel, ^[] Thomas Wågberg^c and Johannes Messinger ^[] ***a.e

Herein, we communicate about an Earth-abundant semiconductor photocathode (p-Si/TiO2/NiOx) as an alternative for the rare and expensive Pt as a counter electrode for overall photoelectrochemical water splitting. The proposed photoelectrochemical (PEC) water-splitting device mimics the "Z"-scheme observed in natural photosynthesis by combining two photoelectrodes in a parallelillumination mode. A nearly 60% increase in the photocurrent density (J_{ph}) for pristine α -Fe₂O₃ and a 77% increase in the applied bias photocurrent efficiency (ABPE) were achieved by replacing the conventionally used Pt cathode with an efficient, cost effective p-Si/TiO₂/NiO_x photocathode under parallel illumination. The resulting photocurrent density of 1.26 mA cm⁻² at $1.23V_{RHF}$ represents a new record performance for hydrothermally grown pristine α-Fe₂O₃ nanorod photoanodes in combination with a photocathode, which opens the prospect for further improvement by doping α -Fe₂O₃ or by its decoration with co-catalysts. Electrochemical impedance spectroscopy measurements suggest that this significant performance increase is due to the enhancement of the space-charge field in α -Fe₂O₃.

Harvesting solar energy to split water into solar fuels such as hydrogen and oxygen by employing catalysts made of Earthabundant elements is the crux of "artificial photosynthesis".^{1–3} Hitherto, extensive research has been performed on designing photoelectrochemical (PEC) water-splitting devices and the respective photocathodes⁴ and photoanodes.⁵ Arranging the photoelectrodes in the parallel-illumination mode replicating the "Z"-scheme of natural photosynthesis⁶ is one option for

employing the abundant solar energy in an effective way.⁷ The major challenges for designing Z-scheme devices include the positioning of the respective band edges so that the conduction band minimum of the photoanode lies at a lower electrochemical potential than the valence band maximum of the photocathode.^{1,8} In addition, finding a favourable aqueous environment for both the photoelectrodes to achieve an efficient PEC performance for long time periods is difficult as most photoanodes are stable at alkaline pH, while the majority of the photocathodes work best at acidic pH.⁹

Recently, Jang et al.10 have reported a tandem PEC device that comprised ZnO/a-Si/TiO₂/Pt as a photocathode and modified hematite (FTO/α-Fe₂O₃-NiFeO_x) as a photoanode. This Ptcontaining device had a solar-to-hydrogen efficiency of 0.91% and thus demonstrated that combining Si and hematite in a tandem device is a promising approach. Tandem PEC devices 10-14 require a semi/transparent front photoelectrode (photoanode) with a wide bandgap energy and a rear photocathode with a narrow band gap energy. Thus, tandem PEC configurations are associated with strict fabrication constraints. 15 On the other hand, the parallel-illumination mode selected in the present study gives the freedom to use opaque photoelectrodes for simultaneous illumination, adding considerable extra flexibility in the device design. We report here a Pt-free device that combines a well-studied pristine α-Fe₂O₃ photoanode16,17 in aqueous 1 M NaOH (pH 13.8; best conditions for α-Fe₂O₃) with a previously optimized micro-structured p-Si/TiO2/NiOx photocathode.18 We demonstrate that this Z-scheme device outcompetes a similar device featuring a Pt cathode. This approach has excellent potential for future optimization since the Earth-abundant Si and Fe₂O₃ photoelectrodes have thermodynamic solar-to-hydrogen conversion capabilities of ~43% and ~15%, respectively. 19

The PEC performance of the pristine $\alpha\text{-Fe}_2O_3$ photoanode was measured (see the ESI† for experimental details) against either a Pt or a microstructured p-Si cathode that was protected by a spin-coated TiO₂ layer and functionalized with a Ni-oxide catalyst (p-Si/TiO₂/NiO_x). These single ($\alpha\text{-Fe}_2O_3$) illumination

^aUmeå University, Department of Chemistry, Sweden.

E-mail: johannes.messinger@kemi.uu.se

^bEuropean Synchrotron Radiation Facility (ESRF), Grenoble, France

^cUmea University, Department of Physics, Sweden

^dUmeå University, Department of Plant Physiology, Umeå Plant Science Centre (UPSC), Umeå, Sweden

^eMolecular Biomimetics, Department of Chemistry, Ångström Laboratory, Unnsala University. Sweden

 $[\]dagger \, \text{Electronic}$ supplementary information (ESI) available. See DOI: 10.1039/c8dt03653e

Dalton Transactions Communication

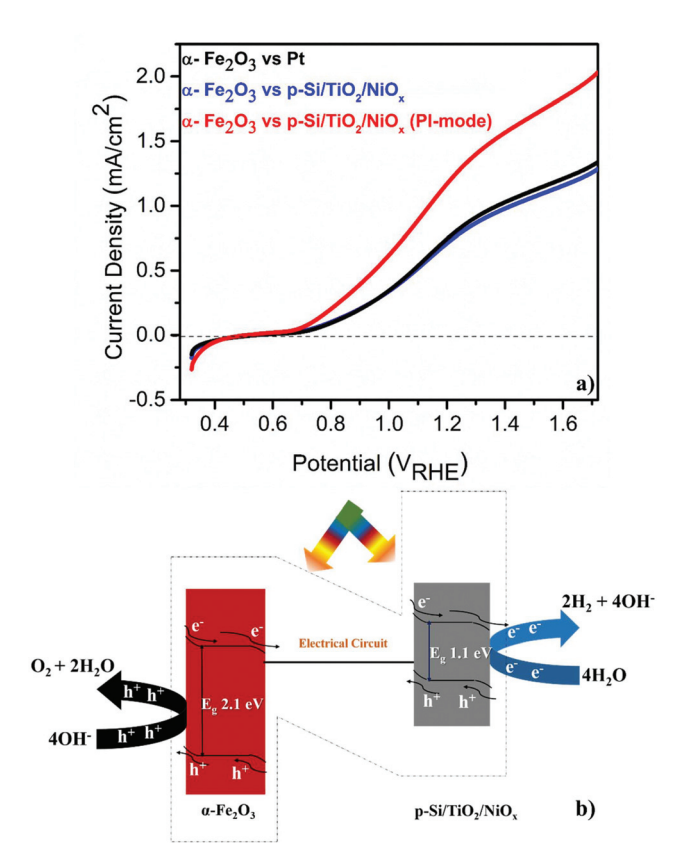


Fig. 1 (a) Linear sweep voltammograms of a pristine α -Fe₂O₃ photo-anode vs. Pt or p-Si/TiO₂/NiO_x in 1 M NaOH (pH 13.8) under standard (1 sun) single or parallel illumination (PI-mode). (b) Schematic band diagram illustrating Z-scheme overall water splitting.

configurations are compared to a Z-scheme configuration, in which the p-Si/TiO2/NiOx electrode was also illuminated at 1 sun and acted as a photocathode (Fig. 1a and b). The detailed and systematic half-cell characterization studies of both photoelectrodes have been presented recently. 16-18 In agreement with these earlier studies, Fig. 1a shows that pristine α-Fe₂O₃ oxidizes, in conjunction with a Pt counter electrode, water with a photocurrent density (J_{ph}) of 0.80 mA cm⁻² in 1 M NaOH (pH 13.8) and $1.23V_{RHE}$. Consistent with the expectation that the hole diffusion length in the pristine α-Fe₂O₃ photoanode limits the overall PEC performance, we found that $J_{\rm ph}$ barely changed (0.77 mA cm⁻²) when p-Si/TiO₂/NiO_x was used instead of Pt and only α-Fe₂O₃ was illuminated. Remarkably, an unprecedented increase in $J_{\rm ph}$ to 1.26 mA cm⁻² was recorded when both α-Fe₂O₃ and p-Si/TiO₂/NiO_x were illuminated simultaneously in the parallel-illumination mode (see the photograph of the PEC cell; Fig. S1†). The elemental and morphological characterization results of the photoelectrodes are shown in Fig. S2 and S3.† Z-scheme illumination is thus an efficient complementary approach for boosting the efficiency of the PEC performance of pristine α-Fe₂O₃. Previous studies have shown performance enhancements of up to ~100% by introducing different dopants^{5,20-22} or suitable underlayers^{23–25} (see Table S1† with the PEC performance of functionalized α-Fe₂O₃ and different electrode assemblies under different illumination conditions). The proposed band energy schematic for overall Z-scheme water splitting is shown in Fig. 1b.1,8 As detailed below, the observed significant increase in the $J_{\rm ph}$ (~60%) in this configuration may be attribu-

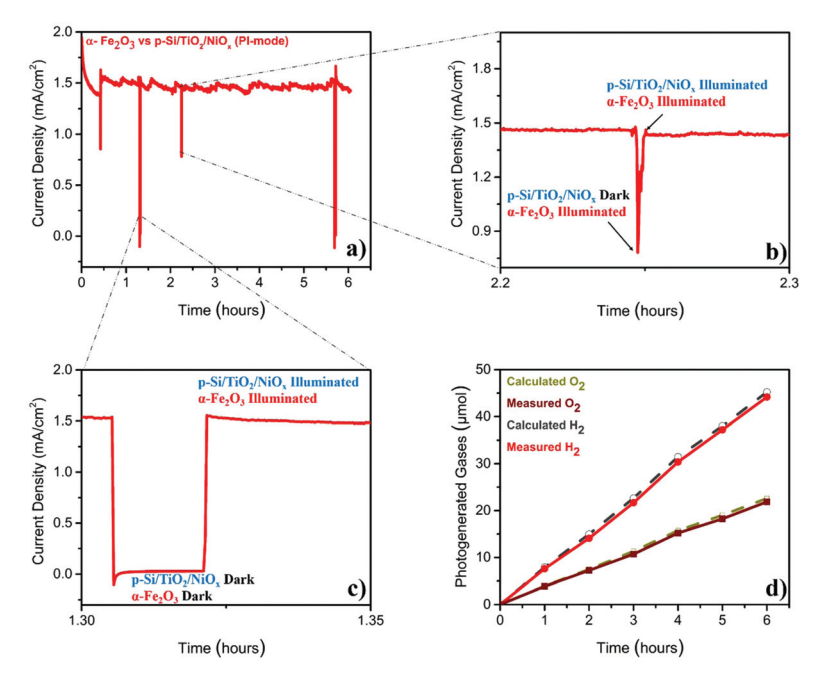


Fig. 2 Photo-electrochemical characterization of α -Fe₂O₃ vs. p-Si/TiO₂/NiO_x in 1 M NaOH (pH 13.8) under standard (1 sun) parallel illumination mode (PI-mode) (a) photocurrent density measured at 1.4V_{RHE}; (b) magnified section showing the photocurrent when only α -Fe₂O₃ is illuminated; (c) magnified section showing the dark current; (d) comparison of calculated and measured photo-generated hydrogen and oxygen (illuminated area of α -Fe₂O₃ was 0.09 cm² and that of p-Si/TiO₂/NiO_x was 0.18 cm²).

ted to the enhanced generation of minority carriers at the p-Si/ TiO₂/NiO_x photocathode, leading to an increased hole-utilization for water oxidation at the surface of the α-Fe₂O₃

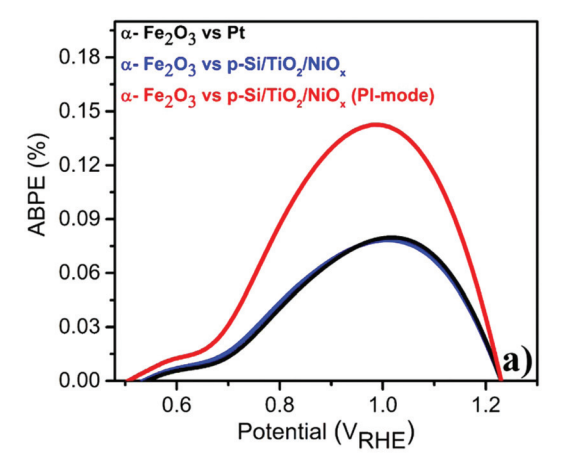
Communication

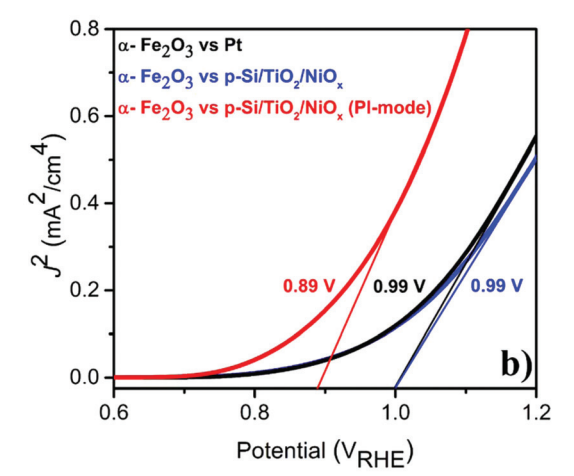
photoanode.

The stability test (Fig. 2a), performed at $1.4V_{\rm RHE}$, demonstrated that the Z-scheme setup operated, after a slight decay in the first 30 min, at a stable photocurrent density of ~1.5 mA cm⁻² over the entire six-hour experiment. The sharp 'spikes' in Fig. 2a were produced by blocking the illumination of the p-Si/TiO₂/NiO_x electrode (Fig. 2b), or of both electrodes (Fig. 2c), demonstrating the photocurrent effects. The gases generated during this parallel-illumination PEC water-splitting experiment were collected and quantified using gas chromatography. The data in Fig. 2d show a stable and stoichiometric light-driven generation of O2 and H2, amounting to ~158 μ mol cm⁻² H₂ and \sim 78 μ mol cm⁻² O₂, which corresponded to a faradaic efficiency of ~96% (the illuminated area of α-Fe₂O₃ was 0.09 cm² and that of p-Si/TiO₂/NiO_x was 0.18 cm²). We additionally examined the photoelectrodes before and after the 6-hour PEC experiment employing X-ray spectroscopy. These high-energy resolution fluorescence detected X-ray absorption near edge structure (HERFD-XANES) and X-ray emission spectroscopy (XES) experiments did not reveal any indications for changes of the photoelectrodes (ESI Fig. S4†).

Given this excellent stability, we determined the applied bias photocurrent efficiencies (ABPE) (Fig. 3(a)), the flat band potentials $(V_{\rm fb})$ (Fig. 3(b)) and the onset potentials $(V_{\rm onset})$ (Fig. 3(c)). In the parallel-illumination mode, a maximum ABPE of ~0.14% was obtained, which is, taking the absorption of additional photons by the p-Si/TiO₂/NiO_x photocathode into account, ~77% higher than that obtained with Pt as the counter electrode. Furthermore, $V_{\rm fb}$ and $V_{\rm onset}$ potentials deduced in the parallel-illumination mode were 100 mV and 40 mV lower as compared to using a Pt counter electrode. These remarkable results further substantiate the idea that the extra holes provided by the p-Si/TiO2/NiOx photocathode increased the hole flux towards water oxidation by enhancing the space-charge region in the α -Fe₂O₃ photoanode. ^{13,26,27} Our observation is in agreement with earlier studies, 28-31 wherein a large enough space-charge region (increased space-charge field) leads to the generation of relatively "long-lived" photogenerated holes that accumulate at the α-Fe₂O₃ electrode surface resulting in increased O₂ evolution.

To test this idea, electrochemical impedance spectroscopy (EIS) was performed. As shown in Fig. 4, replacing the Pt counter electrode by the p-Si/TiO2/NiOx photocathode improved the interfacial charge-transfer kinetics significantly. The charge-transfer resistance (R_{CT2} – larger semicircular region) across the photoanode/electrolyte interface reduced from 439.8 Ω to 298.2 Ω . The 33% decrease in $R_{\rm CT2}$ is attributed to the favorable band edge shifts in both α-Fe₂O₃ and p-Si/TiO₂/NiO_x under parallel illumination leading to a more effective transfer of photoexcited charge carriers to the surface of the respective photoelectrodes. These effective band edge shifts also increased the surface charges of the α-Fe₂O₃ photoanode, thereby allowing for a better surface adsorption of OH⁻





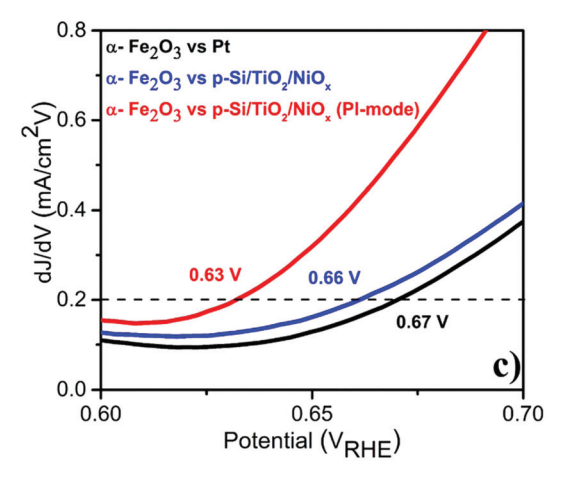


Fig. 3 Photo-electrochemical performance of α -Fe₂O₃ vs. Pt or p-Si/ TiO₂/NiO_x in 1 M NaOH (pH 13.8) under standard (1 sun) single or parallel illumination (PI-mode) derived from LSVs shown in Fig. 1 (a) ABPE (%) (b) flat-band potential ($V_{\rm fb}$) and (c) $V_{\rm onset}$.

onto α-Fe₂O₃, which improved the charge-transfer kinetics at the photoanode/electrolyte interface. However, the Z-scheme configuration also led to an undesired increase in hole recombination losses in the bulk of the α-Fe₂O₃ photoanode, as witDalton Transactions Communication

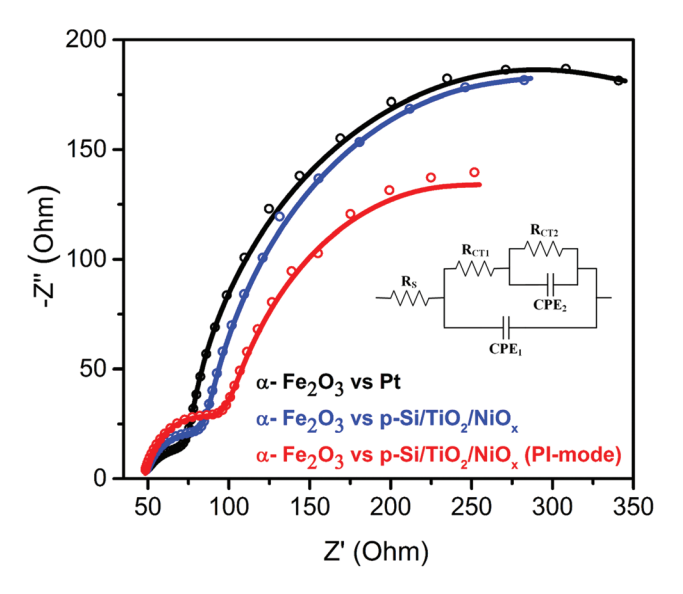


Fig. 4 Nyquist plots of α -Fe₂O₃ vs. Pt or p-Si/TiO₂/NiO_x in 1 M NaOH (pH 13.8) under standard (1 sun) single or parallel illumination (PI-mode). The inset shows the equivalent circuit³⁰ employed for analyzing the Nyquist plots. The fit data are provided in ESI Table S2.†

nessed by the increased intrinsic charge-transfer resistance ($R_{\rm CT1}$ – smaller semicircular region) from 42.09 to 64.26 Ω . This suggests that the sluggish hole mobility in the hematite photoanodes and the resulting recombination losses remained a bottleneck for the overall performance, in agreement with several previous studies. ^{5,27,32} However, such losses may be minimized in the future by using suitable dopants for $\alpha\text{-Fe}_2\mathrm{O}_3$. ^{20,33,34}

Our results demonstrate that aqueous NaOH (pH 13.8) is a favorable environment for both the α -Fe₂O₃ photoanode and the p-Si/TiO₂/NiO_x photocathode, allowing stable Z-scheme device operation for overall light-driven water splitting with significantly better performance as compared to Pt counter electrodes.

Conclusions

A noteworthy photocurrent density $(J_{\rm ph})$ of 1.26 mA cm⁻² at 1.23 $V_{\rm RHE}$ was achieved using a pristine α -Fe₂O₃ photoanode in combination with a micro-structured p-Si/TiO₂/NiO_x photocathode in parallel illumination, clearly outcompeting conventional device designs employing Pt counter electrodes. The micro-structured p-Si/TiO₂/NiO_x photocathode in this Z-scheme configuration improved the charge-transfer kinetics at the α -Fe₂O₃ photoanode/electrolyte interface, but also led to increased bulk recombination. This suggests that this Z-scheme device can be readily improved in future by suitable doping of the α -Fe₂O₃ photoanode and by functionalization with catalysts.

Conflicts of interest

The authors declare no competing financial interest.

Acknowledgements

The authors thank the European Synchrotron Radiation Facility for granting beamtime and the ID 26 beamline staff for the assistance during the experiments. The Knut and Alice Wallenbergs Foundation (Artificial Leaf Project; KAW 2011.0055) provided financial support. T. W. acknowledges support from Vetenskapsrådet (2017-04862), Energimyndigheten (45419-1), and Ångpanneföreningen (15-483).

References

- 1 M. Grätzel, Nature, 2001, 414, 338.
- 2 M. G. Walter, E. L. Warren, J. R. McKone, S. W. Boettcher, Q. Mi, E. A. Santori and N. S. Lewis, *Chem. Rev.*, 2010, **110**, 6446–6473.
- 3 Y. Tachibana, L. Vayssieres and J. R. Durrant, *Nat. Photonics*, 2012, **6**, 511.
- 4 Y. Hou, B. L. Abrams, P. C. Vesborg, M. E. Björketun, K. Herbst, L. Bech, A. M. Setti, C. D. Damsgaard, T. Pedersen and O. Hansen, *Nat. Mater.*, 2011, **10**, 434.
- 5 A. Kay, I. Cesar and M. Grätzel, J. Am. Chem. Soc., 2006, 128, 15714–15721.
- 6 W. Lubitz, E. J. Reijerse and J. Messinger, *Energy Environ. Sci.*, 2008, **1**, 15–31.
- 7 S. Ida, K. Yamada, T. Matsunaga, H. Hagiwara, Y. Matsumoto and T. Ishihara, *J. Am. Chem. Soc.*, 2010, **132**, 17343–17345.
- 8 N. Queyriaux, N. Kaeffer, A. Morozan, M. Chavarot-Kerlidou and V. Artero, *J. Photochem. Photobiol.*, *C*, 2015, **25**, 90–105.
- 9 S. Chen and L.-W. Wang, Chem. Mater., 2012, 24, 3659-3666.
- 10 J.-W. Jang, C. Du, Y. Ye, Y. Lin, X. Yao, J. Thorne, E. Liu, G. McMahon, J. Zhu and A. Javey, *Nat. Commun.*, 2015, 6, 7447.
- 11 Y. Qiu, W. Liu, W. Chen, G. Zhou, P.-C. Hsu, R. Zhang, Z. Liang, S. Fan, Y. Zhang and Y. Cui, *Sci. Adv.*, 2016, 2, e1501764.
- 12 J. Luo, J.-H. Im, M. T. Mayer, M. Schreier, M. K. Nazeeruddin, N.-G. Park, S. D. Tilley, H. J. Fan and M. Grätzel, *Science*, 2014, 345, 1593–1596.
- 13 C. Ding, W. Qin, N. Wang, G. Liu, Z. Wang, P. Yan, J. Shi and C. Li, *Phys. Chem. Chem. Phys.*, 2014, **16**, 15608–15614.
- 14 L. Pan, J. H. Kim, M. T. Mayer, M.-K. Son, A. Ummadisingu, J. S. Lee, A. Hagfeldt, J. Luo and M. Grätzel, *Nat. Catal.*, 2018, 1, 412.
- 15 Y. Kuang, T. Yamada and K. Domen, *Joule*, 2017, **1**(2), 290–305.
- 16 A. Annamalai, A. Subramanian, U. Kang, H. Park, S. H. Choi and J. S. Jang, *J. Phys. Chem. C*, 2015, **119**, 3810–3817.
- 17 A. Annamalai, P. S. Shinde, T. H. Jeon, H. H. Lee, H. G. Kim, W. Choi and J. S. Jang, *Sol. Energy Mater. Sol. Cells*, 2016, **144**, 247–255.
- 18 A. Kawde, A. Annamalai, L. Amidani, M. Boniolo, W. L. Kwong, A. Sellstedt, P. Glatzel, T. Wagberg and J. Messinger, Sustainable Energy Fuels, 2018, 2, 2215–2223.

19 Z. Chen, T. F. Jaramillo, T. G. Deutsch, A. Kleiman-Shwarsctein, A. J. Forman, N. Gaillard, R. Garland, K. Takanabe, C. Heske and M. Sunkara, *J. Mater. Res.*, 2010, 25, 3–16.

Communication

- 20 A. Annamalai, R. Sandström, E. Gracia-Espino, N. Boulanger, J.-F. Boily, I. Mühlbacher, A. Shchukarev and T. Wågberg, ACS Appl. Mater. Interfaces, 2018, 10, 16467–16473.
- 21 A. Y. Ahmed, M. G. Ahmed and T. A. Kandiel, *J. Phys. Chem. C*, 2016, **120**, 23415–23420.
- 22 A. Kay, D. A. Grave, D. S. Ellis, H. Dotan and A. Rothschild, ACS Energy Lett., 2016, 1, 827–833.
- 23 K. Sivula, F. L. Formal and M. Gratzel, *Chem. Mater.*, 2009, 21, 2862–2867.
- 24 A. Annamalai, P. S. Shinde, A. Subramanian, J. Y. Kim, J. H. Kim, S. H. Choi, J. S. Lee and J. S. Jang, *J. Mater. Chem. A*, 2015, 3, 5007–5013.
- 25 I. S. Cho, H. S. Han, M. Logar, J. Park and X. Zheng, Adv. Energy Mater., 2016, 6, 1501840.
- 26 J. Brillet, J.-H. Yum, M. Cornuz, T. Hisatomi, R. Solarska, J. Augustynski, M. Graetzel and K. Sivula, *Nat. Photonics*, 2012, 6, 824.

- 27 P. S. Shinde, S. H. Choi, Y. Kim, J. Ryu and J. S. Jang, *Phys. Chem. Chem. Phys.*, 2016, 18, 2495–2509.
- 28 D. A. Wheeler, G. Wang, Y. Ling, Y. Li and J. Z. Zhang, *Energy Environ. Sci.*, 2012, 5, 6682–6702.
- 29 F. Le Formal, S. R. Pendlebury, M. Cornuz, S. D. Tilley, M. Grätzel and J. R. Durrant, *J. Am. Chem. Soc.*, 2014, 136, 2564–2574.
- 30 T. Lopes, L. Andrade, F. Le Formal, M. Gratzel, K. Sivula and A. Mendes, *Phys. Chem. Chem. Phys.*, 2014, **16**, 16515–16523.
- 31 F. Le Formal, E. Pastor, S. D. Tilley, C. A. Mesa, S. R. Pendlebury, M. Grätzel and J. R. Durrant, *J. Am. Chem. Soc.*, 2015, 137, 6629–6637.
- 32 L. Jia, K. Harbauer, P. Bogdanoff, I. Herrmann-Geppert, A. Ramírez, R. van de Krol and S. Fiechter, *J. Mater. Chem. A*, 2014, 2, 20196–20202.
- 33 W. L. Kwong, C. C. Lee, A. Shchukarev, E. Björn and J. Messinger, J. Catal., 2018, 365, 29–35.
- 34 R. Zhang, Y. Fang, T. Chen, F. Qu, Z. Liu, G. Du, A. M. Asiri, T. Gao and X. Sun, *ACS Sustainable Chem. Eng.*, 2017, 5, 7502–7506.